Observability-based Placement of Inertial Sensors on Robotic Manipulators for Kinematic State Estimation

Michael Fennel, Lukas Driller, Antonio Zea, and Uwe D. Hanebeck

Intelligent Sensor-Actuator-Systems Laboratory (ISAS)
Institute for Anthropomatics and Robotics (IAR)
Karlsruhe Institute of Technology (KIT), Germany
{*firstname*}.{*lastname*}*@kit.edu*

Abstract: In recent years, the demand for accurate and delay-free kinematic state estimates, especially regarding acceleration, led to the adoption of inertial sensors placed along the kinematic chain of robotic manipulators. With state-of-the-art signal processing algorithms, arbitrary setups of accelerometers and gyroscopes can be deployed, raising the question of where and how many sensors should be placed for an optimal estimation quality. This paper presents a novel observability-based approach to answer this question independent of a specific estimator implementation. For this purpose, methods for calculating the required sensor measurement ranges and predicting the estimation quality regarding velocity and acceleration are introduced and discussed. The resulting procedure is validated successfully by comparing predicted and actual estimation quality for two example manipulators, indicating that it can provide meaningful aid to a design engineer.

Keywords: design methodologies, robot manipulators, multisensor systems, observability, data fusion, sensor signal consolidation, perception and sensing, motion control systems

1. INTRODUCTION

A basic requirement for high-precision robot systems is accurate knowledge about the kinematic state composed of joint position, velocity, and acceleration. Especially the latter is required for the application of advanced control schemes, such as Han et al. (2000); Wu et al. (1996); Zimmermann et al. (2020). Unfortunately, pure encoder setups are insufficient for obtaining suitable acceleration estimates as the accuracy is limited in real-time context due to encoder noise and the phase lag of smoothing filters. For this reason, the addition of inertial sensors to manipulators with the goal to improve the quality of kinematic state estimates has become appealing. The algorithms created in this context usually rely on a specific sensor setup or cannot handle arbitrary combinations of gyroscopes and accelerometers as seen in Nori et al. (2018). Just recently, we published a new method (Fennel et al. (2022)) removing any requirements on the placement of the inertial sensors and facilitating superior velocity and acceleration estimates compared to encoder-only setups. While this creates plenty of design opportunities, it raises the question of how an optimal configuration of inertial sensors looks like on a given manipulator, taking into account criteria such as sensor count, measurement range utilization, and estimation quality.

The issue of finding an optimal distribution of sensors is a recurring topic in different engineering domains. For example, Chen and Li (2002) present a method for automatically determining camera poses for optimal visual inspection and Frisch et al. (2022) consider the problem of optimally placing sensors for multilateration. In the context of robot manipulators, Wijayasinghe et al. (2018) study different inertial sensor configurations on a SCARA manipulator to estimate the robot pose when joint encoders are unavailable. Here, the rating is based directly on an estimator's RMS error and hence requires a full simulation pipeline or physical experiments, which is costly for complex manipulators. A very similar approach for the accurate state estimation of the human lower limb is presented by Niswander et al. (2020). The necessity of running the actual state estimator to assess a sensor configuration is eliminated for continuum robots in the work of Mahoney et al. (2016). Instead, the posterior covariance of a Kalman Filter-based estimator is utilized to obtain an expression for the uncertainty of a sensor setup without sensor readings. Unfortunately, this approach is tailored to continuum robots and cannot be transferred easily to serial kinematic chains. Furthermore, only the placement of sensors is optimized but not the actual sensor set. In control theory, the observability of a system is of interest for the selection and placement of sensors, as it provides information about the ability to estimate some variables without necessarily measuring them directly. This idea is also applied in various robotic use cases, such as gripper design (Grossard et al. (2009)) or trajectory planning (Glotzbach et al. (2014)). In the context of kinematic state estimation, a noteworthy contribution was made by Hinson (2014), where the observability Gramian and the observability rank condition are used in applications such as gyroscopic sensing in insect wings. Likewise, Rakhim et al. (2019) use the observability Gramian to optimize the sensor placement and the sensor subset on a

⋆ This work was supported by the ROBDEKON project of the German Federal Ministry of Education and Research.

variable impedance actuated robot. Although this approach is already close to answering the initially stated question, it lacks the ability to focus on velocity and acceleration state information and it overlooks measurement range limitations.

For this reason, we propose a novel sensor placement procedure that is based on the observability Gramian and that facilitates the optimal placement of a pre-defined maximal number of gyroscopes and accelerometers. Beyond that, we assess the sensors' measurement range limits to assist in the selection of suitable sensor locations and types.

2. PRELIMINARIES

Throughout this paper, vectors are printed underlined and matrices are printed in bold. Positions, linear velocities, and linear accelerations are denoted with $\underline{x}$, $\underline{v}$, and $\underline{a}$, respectively. For rotations, rotation matrices $\mathbf{C}$ are used in combination with angular velocities $\underline{\omega}$. Furthermore, $\underline{q}$ is the generalized joint configuration vector. Superscripts denote the resolving coordinate frame in which a quantity is expressed. The subscripts denote the reference frame (if applicable) and the object frame. For example, $\underline{x}^A_{BC}$ represents the position of frame or point C relative to frame B, given in coordinates of frame A. Similarly, $\mathbf{R}^A_B$ describes the orientation of frame B relative to frame A. The kinematic Jacobians $\boldsymbol{\mathcal{J}}_{\underline{v}^W_{WS}}$ and $\boldsymbol{\mathcal{J}}_{\underline{\omega}^W_{WS}}$ relate the joint velocity $\dot{\underline{q}}$ with the linear and the angular velocity through $\underline{v}^W_{WS} = \boldsymbol{\mathcal{J}}_{\underline{v}^W_{WS}} \dot{\underline{q}}$ and $\underline{\omega}^W_{WS} = \boldsymbol{\mathcal{J}}_{\underline{\omega}^W_{WS}} \dot{\underline{q}}$.

To reference the i-th element of a vector, $[i]$ is appended to the subscript. Likewise, $[i,j]$ addresses the i-th row and the j-th column of a matrix. The notation $a{:}b$ is used to express an index range from a to $b-1$. Omitted bounds are equivalent to the natural bounds of the range. In the remainder, the world frame W is considered an inertial frame and marks the stationary base of the robot. All quantities are given in SI units unless otherwise specified.

3. PROBLEM FORMULATION

In this paper, a serial manipulator with known forward kinematics and n joints, which are either prismatic or revolute joints, is considered. Kinematic redundancies are explicitly allowed. Each joint is equipped with an encoder providing absolute but noisy position data with standard deviation σ_E. This way, all kinematic joint quantities are guaranteed to be observable without further instrumentation, independent of singularities and redundancies. It is possible to install zero or more triaxial, noisy inertial sensors along the kinematic chain. Each of these sensors is described by the tuple

$$\mathcal{S} = \left(\mathcal{I}, \sigma, l, \underline{x}^{\beta_l}_{\beta_l S}, \mathbf{C}^{\beta_l}_S\right), \tag{1}$$

whereas $\mathcal{I} \in \{\mathcal{A}, \mathcal{G}\}$ decides whether the sensor mounted at frame S on link $l \in \{1, ..., n\}$ with noise standard deviation σ is an accelerometer or a gyroscope. The placement of S relative to the link is specified using $\underline{x}^{\beta_l}_{\beta_l S}$ and $\mathbf{C}^{\beta_l}_S$ with the link reference frame β_l . The sensor configuration

$$\mathcal{K} = \{\mathcal{S}_1, ..., \mathcal{S}_k\} \tag{2}$$

represents the unique combination of $k \in \mathbb{N}_0$ sensors. All *feasible* sensor configurations with exactly $m = |\mathcal{K}|$ sensors are summarized in the set K_m. With an upper bound of l sensors, the total set of feasible sensor configurations is

$$\bar{K}_l = K_0 \cup K_1 \cup ... \cup K_l \,. \tag{3}$$

As stated in the introduction, the motivation is to estimate the manipulator's kinematic state consisting of joint position $\underline{q}$, velocity $\dot{\underline{q}}$, and acceleration $\ddot{\underline{q}}$ as best as possible with a constrained number of sensors. Thus, the sensor configuration $\mathcal{K}^*$ that minimizes an observability measure J describing the potential estimation uncertainty has to be found. Mathematically, this is equivalent to

$$\mathcal{K}^* = \underset{\mathcal{K} \in \bar{K}_l}{\operatorname{argmin}} \, J(\mathcal{K}) \,. \tag{4}$$

4. PLACEMENT PROCEDURE

The previous problem statement raises two questions. On the one hand, it is unclear which sensor configurations are feasible. On the other hand, a suitable objective function has to be specified. Both questions will be answered in the following, yielding a novel sensor placement algorithm.

4.1 Calculation of Measurement Ranges

For sensor fusion, it is vital that all inertial sensors are exposed to physical values within their measurement ranges. However, the measurement range of sensors cannot be increased arbitrarily without sacrificing resolution or violating device specifications. For this reason, the expected maximal quantity must be evaluated beforehand for each potential sensor position, depending on the expected maximal joint velocities and accelerations as well as the configuration $\underline{q}$. Eventually, suitable sensor types can be identified with the resulting measurement ranges.

Formally, we assume that the set of reachable joint velocities has the shape of an axis-aligned ellipsoid scaled with the maximal joint velocities $\dot{\underline{q}}_{\max}$, i.e.,

$$\left\{\dot{\underline{q}} = \mathbf{D}_{\dot{\underline{q}}} \tilde{\dot{\underline{q}}} \mid ||\tilde{\dot{\underline{q}}}||_2 \leq 1\right\} \text{ with } \mathbf{D}_{\dot{\underline{q}}} = \operatorname{diag}\left(\dot{\underline{q}}_{\max}\right) . \tag{5}$$

Although this does not reflect the reality in the case of fully independent joints, it provides a good approximation as all joints rarely reach their maximal velocity at the same time. Furthermore, it facilitates the calculation of true upper bounds for all inertial sensor measurements as shown below. The set of reachable joint accelerations is defined analogously to (5) with $\mathbf{D}_{\ddot{\underline{q}}} = \operatorname{diag}\left(\ddot{\underline{q}}_{\max}\right)$.

Gyroscope: The angular rate measured at a gyroscope mounted at frame S is given by

$$\underline{\omega}^S_{WS} = \mathbf{C}^S_W \boldsymbol{\mathcal{J}}_{\underline{\omega}^W_{WS}} \dot{\underline{q}} \,. \tag{6}$$

With the definition of the set of feasible joint velocities $\dot{\underline{q}}$, this can be written componentwise as

$$\underline{\omega}^S_{WS[i]} = \left(\mathbf{C}^S_W \boldsymbol{\mathcal{J}}_{\underline{\omega}^W_{WS}} \mathbf{D}_{\dot{\underline{q}}}\right)_{[i,:]} \tilde{\dot{\underline{q}}} . \tag{7}$$

The maximal absolute value of this expression is

$$\underline{\omega}^S_{WS,\max[i]} = \max\left|\underline{\omega}^S_{WS[i]}\right| = \left\| \left(\mathbf{C}^S_W \boldsymbol{\mathcal{J}}_{\underline{\omega}^W_{WS}} \mathbf{D}_{\dot{\underline{q}}}\right)_{[i,:]} \right\|_2 \tag{8}$$

due to the submultiplicativity of the spectral norm and the feasible range of $\tilde{\dot{\underline{q}}}$. Hence, the maximal amplitude over all gyroscope axes is

$$\omega^S_{WS,\max} = \left\|\underline{\omega}^S_{WS,\max}\right\|_\infty . \tag{9}$$

Accelerometer: The necessary calculations for an accelerometer at frame S are more elaborate because the acceleration in world coordinates

$$\underline{a}^W_{WS} = \frac{\partial}{\partial t}\left(\boldsymbol{\mathcal{J}}_{\underline{v}^W_{WS}}\dot{\underline{q}}\right) + \underline{g} = \boldsymbol{\mathcal{J}}_{\underline{v}^W_{WS}}\ddot{\underline{q}} + \frac{\partial}{\partial t}\left(\boldsymbol{\mathcal{J}}_{\underline{v}^W_{WS}}\right)\dot{\underline{q}} + \underline{g} \quad (10)$$

is composed of terms depending on joint accelerations, joint velocities, and gravity $\underline{g}$. If the joint velocity dependant term is considered componentwise, it can be rearranged to

$$\begin{aligned}\left(\frac{\partial}{\partial t}\left(\boldsymbol{\mathcal{J}}_{\underline{v}^W_{WS}}\right)\dot{\underline{q}}\right)_{[i]} &= \frac{\partial^2 \underline{x}^W_{WS[i]}}{\partial \underline{q}\partial t}\dot{\underline{q}} = \dot{\underline{q}}^\mathsf{T}\frac{\partial}{\partial \underline{q}}\left(\frac{\partial \underline{x}^W_{WS[i]}(\underline{q})}{\partial \underline{q}}\right)^\mathsf{T}\dot{\underline{q}} \\ &= \dot{\underline{q}}^\mathsf{T}\mathbf{H}_i\dot{\underline{q}}\end{aligned} \quad (11)$$

using the definition of the Jacobian, Schwarz's theorem, and the chain rule. The occurring Hessian $\mathbf{H}_i$ of $\underline{x}^W_{WS[i]}$ can be calculated as presented by Hourtash (2005) or with an extension of the recursive scheme presented by Fennel et al. (2022).

The resolving frame is changed to S via componentwise transformation yielding

$$\underline{a}^S_{WS[i]} = \underbrace{\left(\mathbf{C}^S_W\boldsymbol{\mathcal{J}}_{\underline{v}^W_{WS}}\right)_{[i,:]}\ddot{\underline{q}}}_{=\underline{\beta}} + \underbrace{\dot{\underline{q}}^\mathsf{T}\tilde{\mathbf{H}}_i\dot{\underline{q}}}_{=\underline{\gamma}} + \underbrace{\mathbf{C}^S_{W[i,:]}\underline{g}}_{=\underline{\delta}} \quad (12)$$

with

$$\tilde{\mathbf{H}}_i = \sum_{j=1}^{3}\mathbf{C}^S_{W[i,j]}\mathbf{H}_i\,. \quad (13)$$

The gravitation-dependant term $\underline{\delta}$ is constant with respect to $\dot{\underline{q}}$ and $\ddot{\underline{q}}$. The influence of the joint acceleration on $\underline{\beta}$ can be handled analogously to the gyroscope in (8), resulting in the componentwise maximal absolute values

$$\underline{\beta}_{\max[i]} = \max\left|\underline{\beta}_{[i]}\right| = \left\|\left(\mathbf{C}^S_W\boldsymbol{\mathcal{J}}_{\underline{v}^W_{WS}}\mathbf{D}_{\ddot{\underline{q}}}\right)_{[i,:]}\right\|_2 . \quad (14)$$

The quadratic term $\underline{\gamma}$ is analyzed with the Courant-Fischer-Weyl min-max principle stating that

$$\lambda_{\min,\mathbf{A}_i}\,\dddot{\underline{q}}^\mathsf{T}\dddot{\underline{q}} \;\le\; \dddot{\underline{q}}^\mathsf{T}\mathbf{A}_i\,\dddot{\underline{q}} \;\le\; \lambda_{\max,\mathbf{A}_i}\,\dddot{\underline{q}}^\mathsf{T}\dddot{\underline{q}} \quad (15)$$

holds for any real symmetric matrix $\mathbf{A}_i \in \mathbb{R}^{n\times n}$ and $\dddot{\underline{q}} \in \mathbb{R}^n$, whereas $\lambda_{\min,\mathbf{A}_i}$ and $\lambda_{\max,\mathbf{A}_i}$ are the smallest and the largest eigenvalue of $\mathbf{A}_i$, respectively. By substituting $\dddot{\underline{q}}$ in $\underline{\gamma}$ according to the set definition (5)

$$\mathbf{A}_i = \mathbf{D}^\mathsf{T}_{\dddot{\underline{q}}}\tilde{\mathbf{H}}_i\mathbf{D}_{\dddot{\underline{q}}} \quad (16)$$

is obtained. With this, the componentwise lower and upper bounds of $\underline{\gamma}$ are easily determined as

$$\underline{\gamma}_{\min[i]} = \begin{cases} 0 & \text{if } \mathbf{A}_i \text{ positive definite} \\ \lambda_{\min,\mathbf{A}_i} & \text{otherwise} \end{cases}, \quad (17)$$

$$\underline{\gamma}_{\max[i]} = \begin{cases} 0 & \text{if } \mathbf{A}_i \text{ negative definite} \\ \lambda_{\max,\mathbf{A}_i} & \text{otherwise} \end{cases}, \quad (18)$$

depending on the definiteness of $\mathbf{A}_i$. Note, that these limits are not overestimating the range of $\underline{\gamma}$ owing to the fact that $\dddot{\underline{q}}$ can reach all normalized eigenvectors of $\mathbf{A}_i$ as well as zero.

Finally, the componentwise limits of $\underline{a}^S_{WS}$ are

$$\underline{a}^S_{WS,\max[i]} = \underline{\beta}_{\max[i]} + \max\left(|\underline{\gamma}_{\min} + \underline{\delta}|_{[i]}, |\underline{\gamma}_{\max} + \underline{\delta}|_{[i]}\right), \quad (19)$$

taking into account that the range of $\underline{\gamma}$ is potentially asymmetric and shifted by $\underline{\delta}$. The overall range of a triaxial accelerometer at frame S is then

$$a^S_{WS,\max} = \left\|\underline{a}^S_{WS,\max}\right\|_\infty . \quad (20)$$

4.2 Observability Measure

Binary statements about the observability as they are often used in control theory (e.g., see Chen (1999)) are not useful in the problem context because a continuous objective function is required. In particular, the assumed sensor setup with encoders at each joint already guarantees full observability of joint velocities and accelerations

To obtain a continuous measure for the observability of the kinematic state

$$\underline{x} = (\underline{q}^\mathsf{T},\, \dot{\underline{q}}^\mathsf{T},\, \ddot{\underline{q}}^\mathsf{T})^\mathsf{T}, \quad (21)$$

we formulate the constant acceleration model

$$\dot{\underline{x}} = \mathbf{A}\underline{x} = \begin{pmatrix} \mathbf{0}_{2n\times n} & \mathbf{I}_{2n\times 2n} \\ \mathbf{0}_{n\times n} & \mathbf{0}_{n\times 2n} \end{pmatrix}\underline{x}, \quad (22)$$

that is initialized at state $\underline{x}_0$ and not affected by noise or inputs. As a result, the acceleration $\ddot{\underline{q}}$ is assumed to be constant. Although this is not true for arbitrary time horizons, it is a reasonable approximation in the case of short time horizons for which we desire to rate the observability. The corresponding measurement equation with dimension $n+3n_g+3n_a$

$$\tilde{\underline{y}}(\underline{x},\mathcal{K}) = \underline{y}(\underline{x},\mathcal{K}) + \underline{v} = \begin{pmatrix} \underline{q} \\ \omega^{G_1}_{WG_1}(\underline{q},\dot{\underline{q}}) \\ \vdots \\ \omega^{G_{n_g}}_{WG_{n_g}}(\underline{q},\dot{\underline{q}}) \\ \underline{a}^{A_1}_{WA_1}(\underline{q},\dot{\underline{q}},\ddot{\underline{q}}) \\ \vdots \\ \underline{a}^{A_{n_a}}_{WA_{n_a}}(\underline{q},\dot{\underline{q}},\ddot{\underline{q}}) \end{pmatrix} + \underline{v} \quad (23)$$

stacks the data from the encoders, from all n_g gyroscopes with the sensing frames G_1 to G_{n_g}, and from all n_a accelerometers with the sensing frames A_1 to A_{n_a} in the considered sensor configuration $\mathcal{K}$. Accordingly, the covariance matrix $\mathbf{R}_\mathcal{K}$ of the additive white Gaussian noise $\underline{v}$ is populated with the sensor covariances σ^2_E, $\sigma^2_{G_i}$, and $\sigma^2_{A_i}$, whose values depend on the sensor types, along its diagonal.

The time-discretization of the already linear system model with sample time Δt yields

$$\underline{x}_{k+l} = \boldsymbol{\Phi}^l\underline{x}_k\,, \quad (24)$$

where $\boldsymbol{\Phi} = \exp(\Delta t\mathbf{A})$ is a constant transition matrix. The measurement model can be linearized using the Jacobian $\mathbf{J}(\underline{x},\mathcal{K}) = \partial\underline{y}(\underline{x},\mathcal{K})/\partial\underline{x}$ utilizing the partial derivatives from Fennel et al. (2022). Now, the definition of the observability Gramian $\mathbf{G}$ for non-linear time-discrete systems from Chen (1999) can be applied, yielding

$$\mathbf{G}(\mathcal{K},\mathcal{T}) = \sum_{k=0}^{M}\left(\boldsymbol{\Phi}^k\right)^\mathsf{T}\mathbf{J}^\mathsf{T}(\hat{\underline{x}}_k,\mathcal{K})\mathbf{R}^{-1}_\mathcal{K}\mathbf{J}(\hat{\underline{x}}_k,\mathcal{K})\boldsymbol{\Phi}^k\,. \quad (25)$$

Here, $\mathcal{T}$ is the reference joint trajectory with samples $\hat{\underline{x}}_k$ and M the time horizon. This definition is closely related to the weighted least squares problem

$$\underline{x}^*_0 = \underset{\underline{x}_0}{\operatorname{argmin}}\sum_{k=0}^{M}\left\|\mathbf{R}^{-\frac{1}{2}}_\mathcal{K}\left(\underline{z}_k - \mathbf{J}(\hat{\underline{x}}_k,\mathcal{K})\boldsymbol{\Phi}^k\underline{x}_0\right)\right\|^2 \quad (26)$$

with

$$\underline{z}_k = \tilde{\underline{y}}(\underline{x}_k,\mathcal{K}) - \underline{y}(\hat{\underline{x}}_k,\mathcal{K}) + \mathbf{J}(\hat{\underline{x}}_k,\mathcal{K})\hat{\underline{x}}_k\,, \quad (27)$$

because the covariance of the estimate $\underline{x}^*_0$ equals the inverse of (25), i.e., $\mathrm{Cov}(\underline{x}^*_0) = \mathbf{G}^{-1}(\mathcal{K},\mathcal{T})$ (see Bar-Shalom et al. (2001)). Thus, the proposed observability Gramian describes

how much *information* can be obtained from a given sensor setup and its inverse describes the *estimation uncertainty*.

Unfortunately, (25) cannot be directly plugged into the optimization problem (4) as $\mathbf{G}(\mathcal{K},\mathcal{T})$ is non-scalar and a robot typically executes more than one trajectory. The first problem can be solved with the construction of a scalar quantity by exploiting the fact that the diagonal elements of the inverse observability Gramian correspond to the mean square estimation error. Hence, we propose two observability measures, where smaller values imply higher observability:

(1) The velocity observability measure corresponds to $h_{\underline{\dot{q}}}(\mathcal{K},\mathcal{T}) = \mathrm{tr}\big((\mathbf{G}^{-1})(\mathcal{K},\mathcal{T})_{[n:2n,n:2n]}\big)$. This way, only uncertainties of velocities are included.
(2) Analogously, a suitable measure for the acceleration observability is defined by $h_{\underline{\ddot{q}}}(\mathcal{K},\mathcal{T}) = \mathrm{tr}\big((\mathbf{G}^{-1})(\mathcal{K},\mathcal{T})_{[2n:,2n:]}\big)$.

A measure that includes the position observability can be constructed as well, but this is usually not of interest in a setup where $\underline{q}$ is directly measured by encoders. To solve the second problem, we propose to simply average over the different elements in the set of trajectories T. Therefore,

$$J(\mathcal{K}) = \frac{1}{|T|}\sum_{\mathcal{T}\in T} h(\mathcal{K},\mathcal{T})\,,\; h\in\big\{h_{\underline{\dot{q}}},h_{\underline{\ddot{q}}}\big\}\,. \tag{28}$$

4.3 Simplifications

So far, the objective function has been specified, but some of the parameters are not yet defined. Furthermore, (4) is a nonlinear mixed-integer problem which is hard, if not impossible, to solve. For this reason, the necessary simplifications are presented in the following.

Time Horizon: For the practical computation of the observability Gramian, the time horizon M must be chosen finite. We propose to set $M=2$ as the presence of the encoders facilitates an acceleration estimation after three measurements in any case, guaranteeing a non-singular observability Gramian. This short horizon also serves as justification for the approximation with a constant acceleration model (22). Moreover, replacing the linearization points $\hat{\underline{x}}_k$ of the trajectory $\mathcal{T}$ with a single linearization point $\hat{\underline{x}}_0$ is now a valid approximation, as only small state changes are to be expected within $2\Delta t$.

Discrete Mounting Points: The definition of the continuous sensor placement (1) is universal but introduces major complexity into the optimization process. Motivated by practical designs, where installation space and thus possible mounting options are limited, we suggest using a set of discrete mounting poses instead of continuous ones. As a result, the placement tuple $(l,\underline{x}_{\beta_l S}^{\beta_l},\mathbf{C}_S^{\beta_l})$ just takes discrete values and the set of feasible configurations K_m becomes finite. When p different placement options exists, m sensors can be mounted in $|K_m| = \binom{2p}{m}$ different combinations. Accordingly,

$$|\bar{K}_l| = \sum\nolimits_{m=0}^{\min(2p,l)} \binom{2p}{m} \tag{29}$$

is the total number of feasible configurations with up to l sensors. For typical robots, (e.g., $p=18$, $l=12$, $|\bar{K}_l|\approx 2.2\times 10^9$), an exhaustive search is computationally costly, but still tractable. Consequently, the solution to problem (4) can be approximated with a combinatorial search. If constructive or economical reasons (e.g., sensors placed only in joints for cost-effectiveness) demand it, the potential sensor mounting points can be reduced. This does not affect the placement procedure in general. However, the resulting estimates tend to be less accurate in general due to the shorter lever arms between joint axes and sensors.

#	configuration $\mathcal{K}$	velocity $h=h_{\underline{\dot{q}}}$		acceleration $h=h_{\underline{\ddot{q}}}$	
		$\log_{10} J$	ranking	$\log_{10} J$	ranking
1	$\{\}$	0.32	11	6.28	11
2	$\{\mathcal{G}$ at $S_1\}$	0.02	9	5.98	10
3	$\{\mathcal{G}$ at $S_2\}$	0.02	8	5.98	9
4	$\{\mathcal{A}$ at $S_1\}$	0.05	10	5.98	7
5	$\{\mathcal{A}$ at $S_2\}$	−0.80	6	−4.05	4
6	$\{\mathcal{G}$ at S_1,$\mathcal{G}$ at $S_2\}$	−4.12	1	1.66	6
7	$\{\mathcal{G}$ at S_1,$\mathcal{A}$ at $S_1\}$	0.02	7	5.98	8
8	$\{\mathcal{G}$ at S_1,$\mathcal{A}$ at $S_2\}$	−1.10	3	−4.05	2
9	$\{\mathcal{G}$ at S_2,$\mathcal{A}$ at $S_1\}$	−1.10	4	1.18	5
10	$\{\mathcal{G}$ at S_2,$\mathcal{A}$ at $S_2\}$	−1.10	2	−4.05	3
11	$\{\mathcal{A}$ at S_1,$\mathcal{A}$ at $S_2\}$	−0.80	5	−4.22	1

Table 1. Evaluation of the proposed observability measures for all feasible sensor configurations in the case of the SCARA manipulator. The notation of $\mathcal{K}$ was simplified for brevity.

Linearization Point: Although a short time horizon removes the need for a fully specified reference trajectory, multiple linearization points are still required. If typical tuples of joint position, velocity, and acceleration are available to the design engineer, these can be used. However, in many cases, this information is not known because it is application dependent. Naïvely sampling over all possible values of $\hat{\underline{x}}_k\in\mathbb{R}^{3n}$ in (28) is an option, but it will quickly become computationally intractable for a higher number of joints. As an alternative, the joint velocity and the joint acceleration in $\hat{\underline{x}}_k$ can be set to $\underline{0}$, which equals a movement starting from standstill. Although this is a rather coarse approximation, we will see that its effect is tolerable in Section 5. The objective (28) therefore collapses to averaging over a set of joint configurations, that can be either derived from typical operating points or sampled from the configuration space under avoidance of irrelevant regions (e.g., kinematic singularities, symmetry).

4.4 Procedure Summary

To obtain an optimized placement of up to l sensors, the following steps must be performed:

(1) Identify a set of suitable sensor mounting poses.
(2) Select a set of typical joint configurations for which to calculate the expected measurement range and the observability measure.
(3) Calculate the expected maximal sensor values according to Section 4.1 for all considered joint configurations and select appropriate sensors, whose noise standard deviations are noted.
(4) Perform the combinatorial search with ranking according to Section 4.2 and Section 4.3.

5. EVALUATION

In the following, the procedure is applied to two examples.

5.1 SCARA Manipulator

For the first example, the placement procedure is applied to a two-joint SCARA manipulator as depicted in Fig. 1(a).

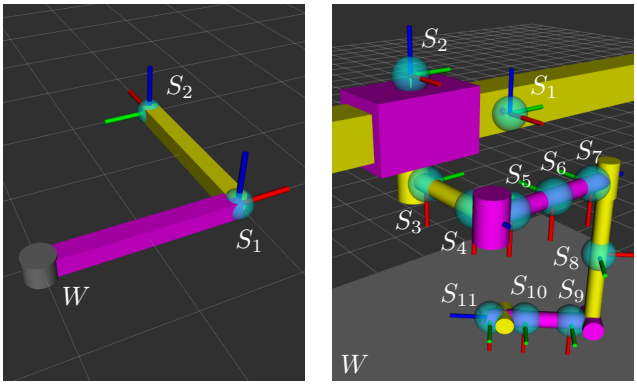

(a) SCARA manipulator. (b) Manipulator with 8 joints.

Fig. 1. Models used for the evaluation of the placement procedure. The potential mounting poses are marked with blue spheres and coordinate systems.

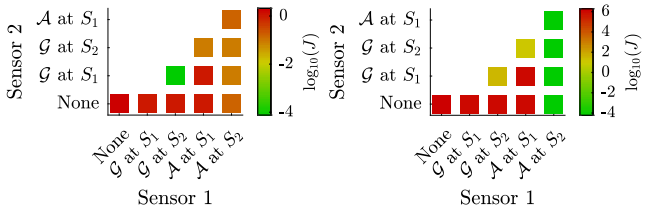

(a) Velocity $h = h_{\dot{q}}$. (b) Acceleration $h = h_{\ddot{q}}$.

Fig. 2. Visualization of the observability measures for all feasible sensor configurations.

Both links have a length of 1 m and a potential mounting point for inertial sensors at their distal ends. To keep the problem comprehensible, only the configuration as shown in Fig. 1(a) is used for the sum (28). This completes step 1 and 2 from Section 4.4.

For step 3, the maximal joint velocity and acceleration are assumed to be $\underline{\dot{q}}_{\max}^{\mathsf{T}} = (180\ \ 180)^\circ\mathrm{s}^{-1}$ and $\underline{\ddot{q}}_{\max}^{\mathsf{T}} = (720\ \ 720)^\circ\mathrm{s}^{-2}$, respectively. This results in a maximal scalar output magnitude $\omega_{WS_1,\max}^{S_1} = 180^\circ\mathrm{s}^{-1}$ for a gyro at S_1 and $\omega_{WS_2,\max}^{S_2} = 255^\circ\mathrm{s}^{-1}$ for a gyro at S_2. Since both sensor frames' z-axes are aligned with the joint axes, this is straightforward to verify. The calculated maximal accelerations at S_1 is $a_{WS_1,\max}^{S_1} = 12.6\mathrm{ms}^{-2}$, which can be verified by calculating gravity, linear, and centripetal acceleration. The maximal acceleration at S_2 is $a_{WS_2,\max}^{S_2} = 32.3\mathrm{ms}^{-2}$ and occurs at $\underline{\dot{q}}^{\mathsf{T}} = (127\ \ 127)^\circ\mathrm{s}^{-1}$, $\underline{\ddot{q}}^{\mathsf{T}} = (720\ \ 0)^\circ\mathrm{s}^{-2}$, as one can verify manually using

$$\underline{a}_{WS_2}^{S_2} = \begin{pmatrix} \ddot{\underline{q}}_{[1]} - (\dot{\underline{q}}_{[1]} + \dot{\underline{q}}_{[2]})^2 \\ \dot{\underline{q}}_{[1]}^2 + \ddot{\underline{q}}_{[1]} + \ddot{\underline{q}}_{[2]} \\ 9.81\mathrm{ms}^{-2} \end{pmatrix}. \tag{30}$$

Consequently, typical MEMS sensors such as the InvenSense MPU-9250 are a suitable choice. The resulting standard deviations at a sampling frequency of 1 kHz are then typically $0.32\,^\circ\mathrm{s}^{-1}$ for gyroscopes, $9.5 \times 10^{-3}\,\mathrm{ms}^{-2}$ for accelerometers, and 0.023° for encoders.

The observability measures from step 4 for all feasible configurations with up to two sensors are listed in Table 1 and visualized in Fig. 2. For an optimal velocity estimate (see Fig. 2(a)), the configuration with gyros at both links should be favored. Combinations with one gyroscope perform much worse because the contributions of both joints cannot be

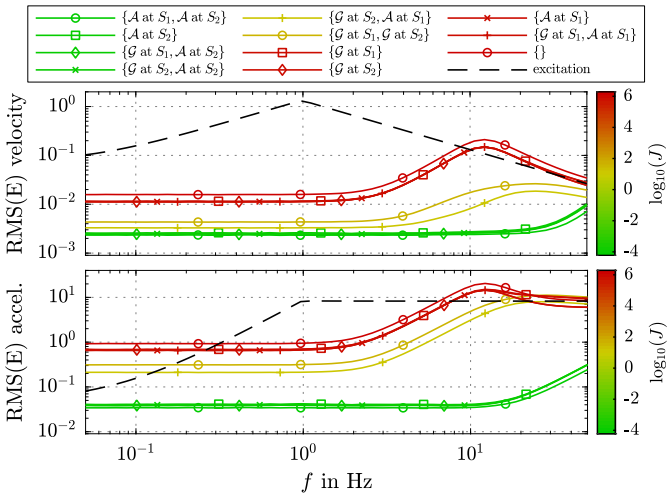

Fig. 3. RMS errors of the studied sensor configurations for the SCARA manipulator. Each setup is colored according to the observability measure J with $h = h_{\ddot{q}}$. The dashed lines represent the RMS values of the excitation signals.

distinguished due to the parallel joint axes. The addition of accelerometers does not improve the velocity estimation significantly, because they only observe velocity changes in the absence of centrifugal and Coriolis accelerations. In contrast to that, an optimal acceleration estimate can be obtained using at least one accelerometer at S_2 according to Fig. 2(b). Here, one accelerometer is already sufficient as both joint accelerations excite a different measurement axis. Interestingly, a second accelerometer at S_1 does not increase the observability score much according to Table 1. If an accelerometer at S_2 is excluded, medium-quality acceleration estimates can be obtained using either two gyros or using one gyro and one accelerometer at different joints. These findings match with what one might expect based on an engineer's intuition: It is beneficial to measure a kinematic quantity without the need for differentiation or integration. Furthermore, one triaxial sensor can sense multiple joints very well as long as the resulting sensor excitations are orthogonal.

To test the meaningfulness of the previous results, all sensor configurations and their acceleration observability scores were analyzed with the IMU-based kinematic state estimator from Fennel et al. (2022). The associated simulation includes sensor errors such as bias, noise, and quantization, but not scale-factor errors or placement errors as these can distort the estimator performance. Fig. 3 depicts the resulting RMS errors for acceleration and velocity. The estimation quality across a large range of frequencies is strongly correlated with the acceleration measure. Even the ranking from the last column of Fig. 1 is reflected for close scores. Interestingly, the acceleration ranking is also valid for ranking the velocity estimation. This is caused by the fact that the used estimator always has a previous velocity estimate allowing the integration of acceleration signals, which stands in contrast to the assumption of the weighted least square problem without prior knowledge from (26). Despite this explainable discrepancy, these results endorse the simplifications from Section 4.3 regarding time horizon, linearization point, and averaging of joint configurations.

at frame	S_1	S_2	S_3	S_4	S_5	S_6	S_7	S_8	S_9	S_{10}	S_{11}
Gyroscope	0.0	0.0	6.0	6.0	8.4	8.4	8.4	11.5	11.5	11.5	16.1
Accelerometer	9.8	9.8	9.8	21.3	25.1	36.5	53.0	59.1	53.7	53.5	65.2

Table 2. Calculated maximal sensor values for the potential mounting poses on the manipulator with 8 joints.

# of sensors	configuration $\mathcal{K}$	$\log_{10} J$
0	{}	6.89
1	{$\mathcal{A}$ at S_{11}}	6.66
2	{$\mathcal{G}$ at S_{11},$\mathcal{A}$ at S_{10}}	6.28
3	{$\mathcal{G}$ at S_{11},$\mathcal{A}$ at S_2,S_{10}}	1.65
4	{$\mathcal{G}$ at S_{11},$\mathcal{A}$ at S_2,S_{10},S_{11}}	1.18
5	{$\mathcal{G}$ at S_{11},$\mathcal{A}$ at S_2,S_9,S_{10},S_{11}}	1.18
6	{$\mathcal{G}$ at S_{11},$\mathcal{A}$ at S_2,S_5,S_9,S_{10},S_{11}}	1.18
14*	{$\mathcal{G}$ and $\mathcal{A}$ at S_1,S_2,S_4,S_7,S_8,S_{10},S_{11}}	1.18

Table 3. Observability measures with $h = h_{\ddot{q}}$ for the best configuration with a given number of sensors. For comparison, a non-optimal configuration with a total of 14 sensors (∗) was added.

5.2 Manipulator with 8 Joints

To demonstrate the effectiveness of the proposed placement procedure for complex manipulators, whose properties cannot be deduced by hand without great effort, we used the kinematic chain from Fig. 1(b) with 2 prismatic and 6 revolute joints. Following the steps from Section 4.4, we first selected suitable mounting poses at each link. As depicted in Fig. 1(b), mounting poses that are fully translation invariant to existing mounting poses were omitted (e.g., S_8 can be shifted up or down arbitrarily). For step 2, the shown configuration was augmented with 80 configurations, where joint 3 varies ±45.0° and joints 4 to 6 vary ±22.5° as this is the typical operation range for the studied manipulator according to Fennel et al. (2021). With the assumption, that the maximal joint velocities and accelerations are $\underline{\dot{q}}_{\max}^{\mathsf{T}} = (1.5 \quad 1.5 \quad 6.0 \quad 6.0 \quad 7.9 \quad 7.9 \quad 14.0 \quad 14.0)$ and $\underline{\ddot{q}}_{\max}^{\mathsf{T}} = (6.0 \quad 6.0 \quad 12.6 \quad 12.6 \quad 12.6 \quad 12.6 \quad 12.6 \quad 12.6)$, the measurement ranges from Table 2 are obtained in step 3. From this, it is clear that a measurement range with $\pm 1000°\mathrm{s}^{-1}$ and $\pm 8\mathrm{ms}^{-2}$ is a reasonable selection criterion for gyroscope and accelerometers, respectively.

According to (29), 110056 sensor combinations are possible with up to six sensors. For this reason, Table 3 only lists the best configuration for each number of sensors. Interestingly, already four sensors at suitable positions are sufficient to minimize the observability measure. Additionally, the last entry of the table indicates that even placing a gyroscope and an accelerometer at the end of each link, which increases the number of sensors to 14, yields no improvement regarding acceleration observability. Although these results might look counterintuitive at the first glance, they match the behavior of the IMU-based kinematic state estimator from the previous chapter as shown in Fig. 4. Hence, the proposed algorithm is meaningful even for complex problems and facilitates the prediction of the estimation quality of a functioning estimator.

6. CONCLUSION

As shown in the evaluation, the presented placement procedure is a helpful tool for finding an optimal inertial sensor configuration in the context of kinematic state estimation. Experiments with a real-world state estimator revealed

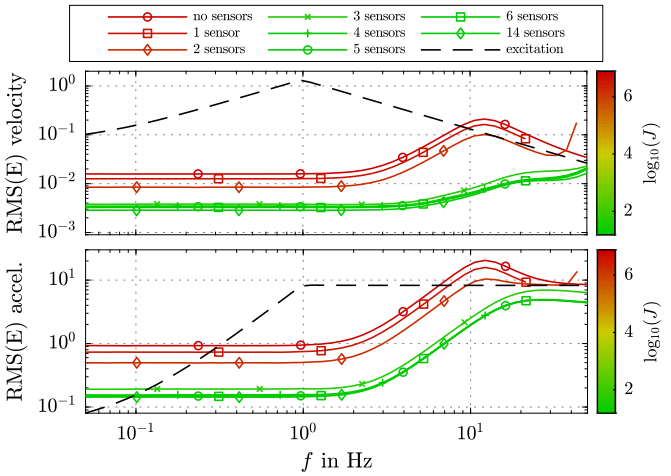

Fig. 4. RMS errors for the manipulator with 8 joints analog to Fig. 3. Note, that the outlier and the missing samples for 1 and 2 sensors are caused by numerical instabilities of the underlying estimator and therefore are unrelated to the placement procedure.

that especially the proposed observability measure for the acceleration is a meaningful quantity to judge the expected estimation quality of a sensor setup. Furthermore, our placement procedure supports the design engineer by finding good solutions, that might be hard to discover manually, and by providing upper bounds for the measurement ranges, which are helpful for the sensor selection.

In future work, we plan to remove some of the simplifications made above, especially the assumption of discrete mounting poses. Although we already demonstrated the practical relevance, we would also like to add some proofs to establish a mathematically sound basis. Furthermore, the examination of related problems, such as finding the worst and best joint configuration for a given sensor setup, is of interest. Manipulator motions are often planned and executed in Cartesian space. This raises the question, whether a Cartesian formulation of the presented placement procedure is feasible and meaningful. Another interesting question, which returns to the design of a suitable state estimator and therefore is beyond the scope of this paper, is how joint torque measurements can be used in combination with the robot dynamics to obtain even better kinematic state estimates.

REFERENCES

Bar-Shalom, Y., Li, X.R., and Kirubarajan, T. (2001). *Estimation with Applications to Tracking and Navigation: Theory Algorithms and Software.* Wiley, New York.

Chen, C.T. (1999). *Linear System Theory and Design.* Oxford Univ. Press, New York, 3rd edition.

Chen, S. and Li, Y. (2002). A method of automatic sensor placement for robot vision in inspection tasks. In *Proc. of the 2002 IEEE Intl. Conf. on Robotics and Automation*, 2545–2550.

Fennel, M., Driller, L., Zea, A., and Hanebeck, U.D. (2022). Calibration-free IMU-based kinematic state estimation for robotic manipulators. In *Proc. of the 2022 IEEE Intl. Conf. on Multisensor Fusion and Integration for Intell. Systems (MFI 2022).* To appear.

Fennel, M., Zea, A., and Hanebeck, U.D. (2021). Optimization-driven design of a kinesthetic haptic

interface with human-like capabilities. *IEEE Trans. on Haptics*, 15(1), 45–50.

Frisch, D., Li, K., and Hanebeck, U.D. (2022). Optimal Sensor Placement for Multilateration Using Alternating Greedy Removal and Placement. In *Proc. of the 2022 IEEE Intl. Conf. on Multisensor Fusion and Integration for Intell. Systems (MFI 2022)*. To appear.

Glotzbach, T., Crasta, N., and Ament, C. (2014). Observability analyses and trajectory planning for tracking of an underwater robot using empirical gramians. *IFAC Proceedings Volumes*, 47(3), 4215–4221.

Grossard, M., Rotinat-Libersa, C., Chaillet, N., and Boukallel, M. (2009). Mechanical and control-oriented design of a monolithic piezoelectric microgripper using a new topological optimization method. *IEEE/ASME Transactions on Mechatronics*, 14(1), 32–45.

Han, J., Wang, Y., Tan, D., and Xu, W. (2000). Acceleration feedback control for direct-drive motor system. In *Proceedings of the 2000 IEEE/RSJ International Conference on Intelligent Robots and Systems(IROS)*, 1068–1074.

Hinson, B.T. (2014). *Observability-Based Guidance and Sensor Placement*. Ph.D. thesis, Univ. of Washington.

Hourtash, A. (2005). The kinematic hessian and higher derivatives. In *Proc. 2005 Intl. Symp. on Comput. Intell. in Robotics and Automation*, 169–174.

Mahoney, A.W., Bruns, T.L., Swaney, P.J., and Webster, R.J. (2016). On the inseparable nature of sensor selection, sensor placement, and state estimation for continuum robots or "where to put your sensors and how to use them". In *2016 IEEE Intl. Conf. on Robotics and Automation (ICRA)*, 4472–4478.

Niswander, W., Wang, W., and Kontson, K. (2020). Optimization of IMU sensor placement for the measurement of lower limb joint kinematics. *Sensors*, 20(21), 5993.

Nori, F., Traversaro, S., and Fallon, M. (2018). Sensor fusion and state estimation of the robot. In A. Goswami and P. Vadakkepat (eds.), *Humanoid Robotics: A Reference*. Springer, Dordrecht.

Rakhim, B., Zhakatayev, A., Adiyatov, O., and Varol, H.A. (2019). Optimal sensor placement of variable impedance actuated robots. In *Proc. of the 2019 IEEE/SICE Intl. Symp. on System Integration*, 141–146.

Wijayasinghe, I.B., Saadatzi, M.N., Abubakar, S., and Popa, D.O. (2018). A study on optimal placement of accelerometers for pose estimation of a robot arm. In *2018 IEEE Intl. Conf. on Robotics and Automation (ICRA)*, 1444–1451.

Wu, Y., Tarn, T.J., Xi, N., and Isidori, A. (1996). On robust impact control via positive acceleration feedback for robot manipulators. In *Proceedings of IEEE International Conference on Robotics and Automation*, 1891–1896.

Zimmermann, Y., Küçüktabak, E.B., Farshidian, F., Riener, R., and Hutter, M. (2020). Towards dynamic transparency: Robust interaction force tracking using multi-sensory control on an arm exoskeleton. In *2020 IEEE/RSJ International Conference on Intelligent Robots and Systems (IROS)*, 7417–7424.